Journal of Materials Chemistry C

COMMUNICATION

View Article Online
View Journal | View Issue

Cite this: J. Mater. Chem. C, 2018, 6, 4866

Received 10th March 2018,
Accepted 16th April 2018

DOI: 10.1039/c8tc01183d

rsc.li/materials-c

Three-dimensional helical inorganic thermoelectric generators and photodetectors for stretchable and wearable electronic devices†

Xiaojie Xu,‡[a] Yong Zuo,‡[a] Sa Cai,[b] Xin Tao,[b] Zhiming Zhang,[b] Xufeng Zhou,[a] Sisi He,[a] Xiaosheng Fang *[b] and Huisheng Peng *[a]

Stretchable, light-weight and breathable thermoelectric generators (TEGs) are highly desired for wearable electronic devices as promising power sources. However, it remains challenging to realize high-performance stretchable TEGs where the employment of inorganic materials is inevitable. Here, we provide the first three-dimensional helical inorganic TEG which is highly stretchable (~100% strain), stable (1000 cycles of stretching), light-weight and breathable, thus indicating its great potential as a portable and wearable power supply that harvests energy from the human body. More importantly, we propose a novel, versatile and effective strategy which artfully transforms rigid electronic devices to stretchable helical ones. This ingenious and general approach for developing various functional wearable electronic devices is further exemplified by ZnO photodetectors, which are also demonstrated as highly stretchable (~600% strain), deformable and breathable. The intelligent architecture design and assembly technique reported in this work will aid in pushing wearable electronic devices a step forward.

Introduction

The trend of "next-generation" electronics is flexible, stretchable and wearable.[1–6] The exciting future beyond conventional rigid wafers and circuit boards has attracted great attention from both academia and industry.[7–10] Intelligent architecture designs and assembly techniques will aid in transforming rigid materials/devices into flexible and stretchable ones that meet the desire of portable and wearable electronic devices.[11,12]

Thermoelectric generators (TEGs), which harvest energy from a temperature gradient, are considered to be one of the most promising power sources for multifunctional wearable electronic systems as a human body is a permanent heat source.[13–15] There are three important technical drivers for a wearable TEG. (1) The thermoelectricity must be generated from the temperature difference between human skin and ambient temperature. (2) The TEG should be mechanically durable above 30% strain due to the dynamic motions carried out by a living body (*e.g.*, bending, stretching and folding).[16–18] (3) For wearable applications, it should be breathable.

With these points in mind, researchers have explored intrinsically flexible organic thermoelectric materials in the construction of wearable TEGs. However, such devices generally suffer from a low output efficiency due to the poor thermoelectric properties of organic materials. It is inevitable to use inorganic materials to realize high performance TEGs.[19–25] To date, very few reports on stretchable inorganic TEGs have been found in the literature,[26,27] such as a recent study by Rojas *et al.*[27] in which a stretchable coil-shaped TEG was fabricated *via* sophisticated laser-cutting and printing processes. However, such a device is hard to be a wearable TEG as its free-standing direction doesn't align with the temperature gradient formed at the human skin–environment interface. In short, a stretchable, breathable, wearable high-performance TEG that meets the three requirements mentioned above hasn't been demonstrated yet.

A three-dimensional helical design is of particular interest due to the very high mechanical strain it can bear,[28] especially if brittle materials are constructed on the surface of the helical architecture, as illustrated in Fig. 1a. More importantly, air permeability and heat preservation, which are generally considered to be two competing processes in wearable TEGs, can be artfully kept in balance in this design, where the gaps between each loop provide breathability, while the air in the loop may serve as a good thermal insulator to minimize the heat transfer from bottom to top of the three-dimensional helical structure. In addition, a versatile and effective assembly technique is urgently desired as it remains a great challenge to directly make devices on three-dimensional helical substrates.

With those objectives in mind, for the first time, a high-performance stretchable, light-weight, breathable and wearable

[a] State Key Laboratory of Molecular Engineering of Polymers, Department of Macromolecular Science, and Laboratory of Advanced Materials, Fudan University, Shanghai 200438, China. E-mail: penghs@fudan.edu.cn
[b] Department of Materials Science, Fudan University, Shanghai 200438, China. E-mail: xshfang@fudan.edu.cn

† Electronic supplementary information (ESI) available. See DOI: 10.1039/c8tc01183d

‡ These authors contributed equally to this work.

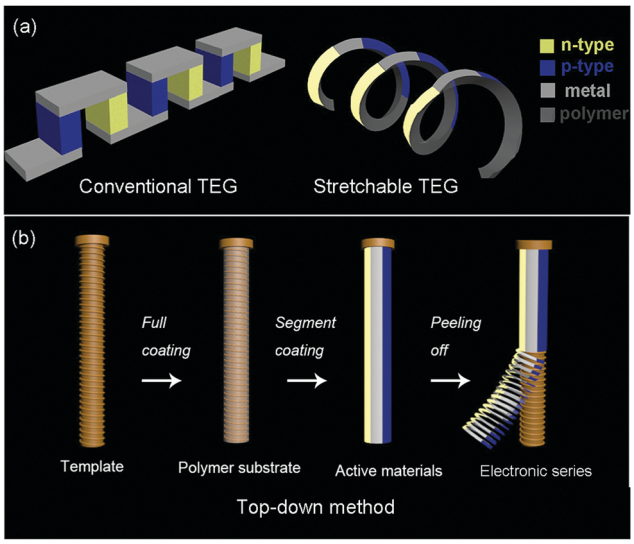

Fig. 1 Schematic illustration of the structure design and assembly technique of three-dimensional helical TEGs. (a) Comparison of the configurations of a conventional TEG and our stretchable helical TEG. (b) The novel "top-down" method to obtain helical inorganic electronic devices that are highly stretchable, breathable and wearable based on the template of a simple screw.

TEG based on a three-dimensional helical design was demonstrated. It could bear strains of up to ~100% and remained perfectly stable after 1000 stretching cycles (strain of ~60%). More importantly, we propose a novel, versatile and facile template method that artfully transforms rigid devices into helical ones by simply peeling them off a screw. Furthermore, it can be easily implemented in other inorganic electronic devices, exemplified by ZnO photodetectors which also exhibit an ultrahigh stretchability (~600% strain) and deformability. This work not only demonstrates a promising wearable power generator that harvests energy from the human body, but also provides a simple, general and effective strategy for developing next-generation stretchable and wearable electronic devices with high performance.

Experimental

Preparation of polymer substrates

Polyurethane (PU) was dissolved in *N*,*N*-dimethylformamide to obtain a viscous polymer solution, and then was filled into the pitch of the screws and dried naturally to form a substrate.

Fabrication of stretchable thermoelectric devices

The thermoelectric materials Bi_2Te_3 (from Aladdin) or Bi_2Se_3 (from Aladdin) powders were mixed with homemade polyvinylidene fluoride (PVDF) binder to form pastes. The two different pastes were coated on a PU substrate on the opposite sides. The films in the screw were dried at 80 °C for 15 min to remove the organic solvent. Conductive silver paste (from Sigma-Aldrich) was then coated onto the gap between the p-type and n-type materials for connection. Afterwards, silver paste was dried in an oven at 80 °C for about 10 min. Finally, the TE device was peeled off the screw carefully with the help of tweezers or blades (Fig. S1, ESI†).

Fabrication of stretchable photodetectors

Polydimethylsiloxane (PDMS) (from Wacker) elastomer base and a curing agent were mixed and half-cured. ZnO nanoparticles (diameter of 30 nm) were uniformly spread and attached on the surface of the half-cured PDMS substrate. Then, the pre-treated screw was immersed in mixed solutions of zinc nitrate hexahydrate ($Zn(NO_3)_2{\cdot}6H_2O$, 0.025 mol L^{-1}) and methenamine ($C_6H_{12}N_4$, 0.025 mol L^{-1}) and kept in a hydrothermal reactor at 80 °C for 5 h. Afterwards, the screw with the deposition of ZnO nanostructures was rinsed with deionized water several times and dried in an oven box, followed by coating Ag paste on the designated area of the substrate to connect ZnO. After carefully peeling the substrate off the screw thread, a helical ZnO photodetector series was obtained.

Characterization

For *I*–*V* and *I*–*t* measurements, ZnO photodetectors, a Keithley 4200-SCS, and a 24 W xenon lamp with a monochromator were used. To investigate the TEG output characteristics, a homemade temperature difference system was set up (Fig. S4, ESI†). The hot side could be controlled by the heating stage, and the aluminum cooling pad was selected as the cold side to obtain the temperature difference, which was monitored with thermocouples all the time. The output voltage and power were measured using an electrochemical workstation (CHI 660D). The thermal images were taken using an infrared camera (PI 450, Optris). The structures were investigated using a field emission scanning electron microscope (S-4800, Hitachi) operated at 1 kV. The photographs were taken using a digital camera (700D, Canon).

Simulation of the local strain distributions

The model was built with finite element software ABAQUS. In this model, one end was fixed in all directions, while the other end was moved by 8.4 mm along the length direction (100%), which was the original length of the structures. The calculated hexagonal mesh size was about 0.2 mm.

Results and discussion

It all started with a simple screw and an ingenious idea, as illustrated in Fig. 1b. Polyurethane, which is typically used as the soft substrate in flexible inorganic electronics, was coated on the screw thread to form a continuous and smooth layer as the platform for further device fabrication. Active materials, including p-type and n-type TE materials, were sequentially coated on the opposite sides of the continuous polymer substrate, and then connected *via* Ag paste. Finally, by peeling off the substrate along the screw thread, a three-dimensional helical stretchable TEG series was achieved. It is worth mentioning that p-type and n-type thermal legs were naturally joined in sequence by metal contact after the peeling method.

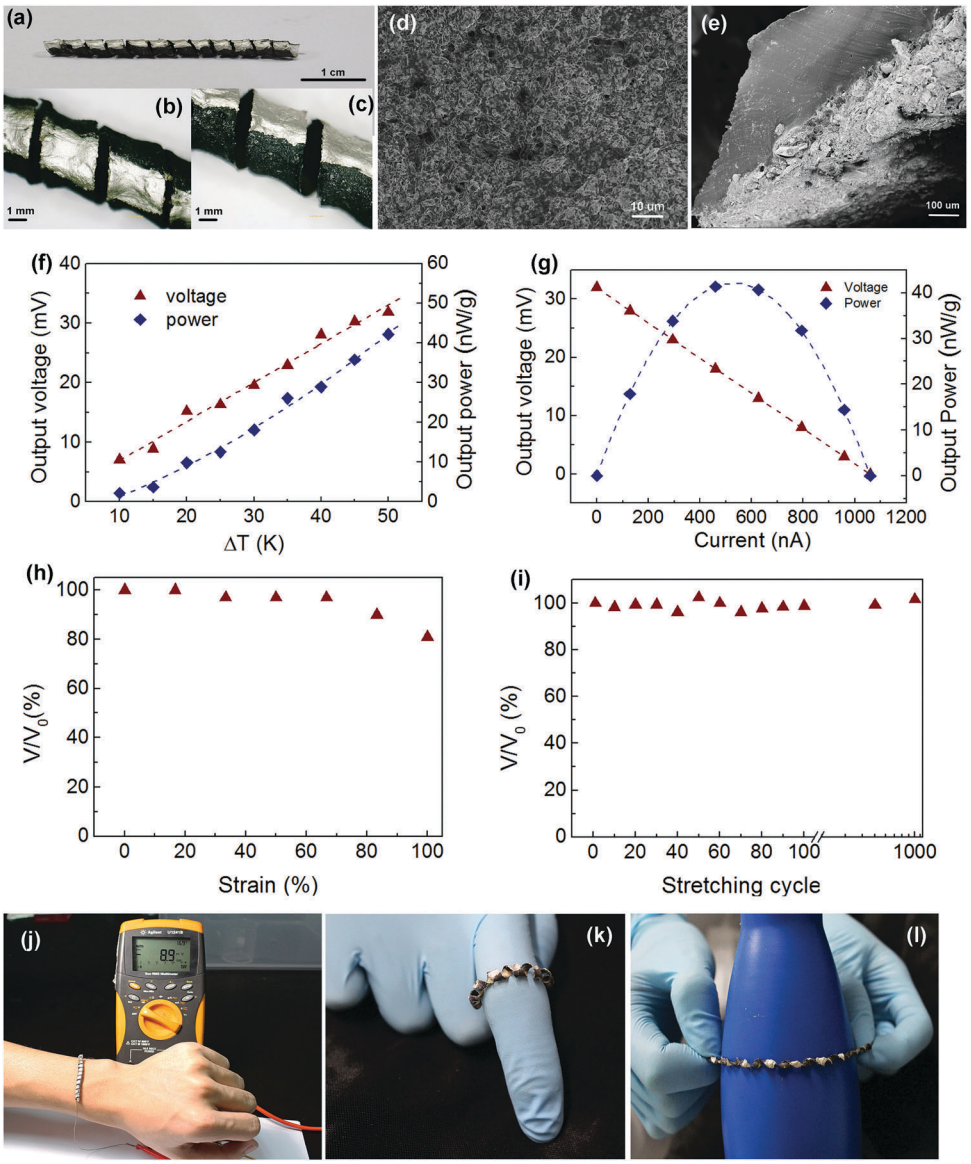

Fig. 2 Photographs, thermoelectric and mechanical performances and simple demonstrations of the as-prepared stretchable helical TEGs. (a) Photograph of a stretchable helical TEG. (b and c) Photographs of the surface and interface of TE films and the Ag interconnect, respectively. (d) SEM image and (e) cross-sectional SEM image of a p-type Bi_2Te_3 film on the PU substrate. (f) Output voltage and power of a helical TEG as functions of ΔT at rest. (g) Output voltage and power of a TEG as functions of current at ΔT = 50 K. (h) Output voltage of the stretchable TEG at a ΔT of 15 K under increasing strains from 0 to 100%. (i) Variations of the output voltage of the stretchable TEG at a ΔT of 15 K after 1000 stretching cycles (strain of ~60%). (j) Photograph of a helical TEG worn on the arm, with an output voltage of 8.9 mV generated at an ambient temperature of ~16 °C. (k and l) Photographs of a stretchable TEG worn on a finger and attached to the cambered surface of a hot cup, respectively.

A prototype comprising a thin layer of inorganic TE materials and Ag on the PU substrate and arranged in sequence is demonstrated in Fig. 2a. Here, some of the best-performing TE materials were used: p-type Bi_2Te_3 and n-type Bi_2Se_3. To form a compact film of Bi_2Te_3/Bi_2Se_3 on the PU substrate, a suitable polymer binder, which will not only hold the Bi_2Te_3 particles tightly together to ensure the thermoelectric and electrical properties of the TE films, but also need to form a good adhesion with the PU substrate, was selected because the actual efficiency of a TEG under real-life operating conditions depends on the entire thermal design of the devices, including the thermal conductivity of every component and length of TE legs.[29]

In this case, PVDF was used as the binder. As can be seen in Fig. 2b and c, the surfaces of the Bi_2Te_3 and Bi_2Se_3 films were smooth and the interfaces of TE films and Ag electrodes were clear, neat and well-connected even after the peeling process, which benefits from the template method as the screw pitches allow for an easy exfoliation of the polymer substrate. No cracks in the Bi_2Te_3 film could be observed even at a micrometer scale, as displayed in Fig. 2d, suggesting that the Bi_2Te_3 particles were tightly held together into a compact film by the PVDF binder. In addition, the cross-sectional SEM images of a thin layer of p-type Bi_2Te_3 and n-type Bi_2Se_3 on the PU substrate are shown in Fig. 2e and Fig. S2 (ESI†). As can be seen, they were firmly bonded.

This is because the solvent *N*,*N*-dimethylformamide in PVDF binder may infiltrate into the PU substrate during the drying process, ensuring the well-interacting interface of the TE film and the PU substrate.

A prototype of a three-dimensional helical TEG series with a few couples of TE legs was studied for its thermoelectric and mechanical performances. As can be seen in Fig. 2f, the output voltage shows a linear relationship with the temperature difference, and the open-circuit voltage reached up to 32 mV when ΔT was $\sim$50 K owing to the comparative temperature difference formed at both ends of the spring-shaped TE legs. The Seebeck coefficients of the p-type Bi_2Te_3 and n-type Bi_2Se_3 films formed by the inorganic TE particles and polymer binder are $\sim$187 $\mu V\ K^{-1}$ and $\sim$79 $\mu V\ K^{-1}$, respectively. The power per unit weight was proportional to the square of ΔT ($P_{MAX} = nS^2(\Delta T)^2/4R$, where n is the number of thermocouples in series, S is the Seebeck coefficient and R is the internal electrical resistance of the TEG).[30,31] Even though the values can't rival those of state-of-the-art TEGs, given the fact that no optimization of the TE particles/PVDF composite films is carried out, various promising improvements can be envisioned by increasing the electrical conductivity of the films. The output voltage and power of the TEG as functions of current under a steady-state temperature difference of 50 K are shown in Fig. 2g. The maximum output power per unit weight is approximately 42 nW g^{-1}, which can be further enhanced by reducing the internal resistance of the device by adjusting the composition of the binder.

The mechanical stability of our stretchable TE generators was studied at a ΔT of 15 K (Fig. 2h). The output voltages remained stable at an applied strain of $\sim$65%, and only a tiny decrease was observed upon further increasing the strain to 100%, which might have resulted from the reduced temperature difference when the TE legs were over-stretched into the horizontal direction. The output powers showed a slight change during the stretching process, suggesting the robustness of the device (Fig. S3a, ESI†). To verify the long-term stability of the TE module, a simple cycling test at a strain of 60% was performed (Fig. 2i). The output voltages were invariable even after 1000 stretching cycles, and the output powers also remained unchanged (Fig. S3b, ESI†). These results indicate that the ingenious three-dimensional helical TEG may work as a promising stretchable and wearable power supply. For demonstration of the use of our stretchable TEG in real life, such a device was simply attached onto the human skin, and a stable open-circuit voltage of 8.9 mV was generated from the temperature

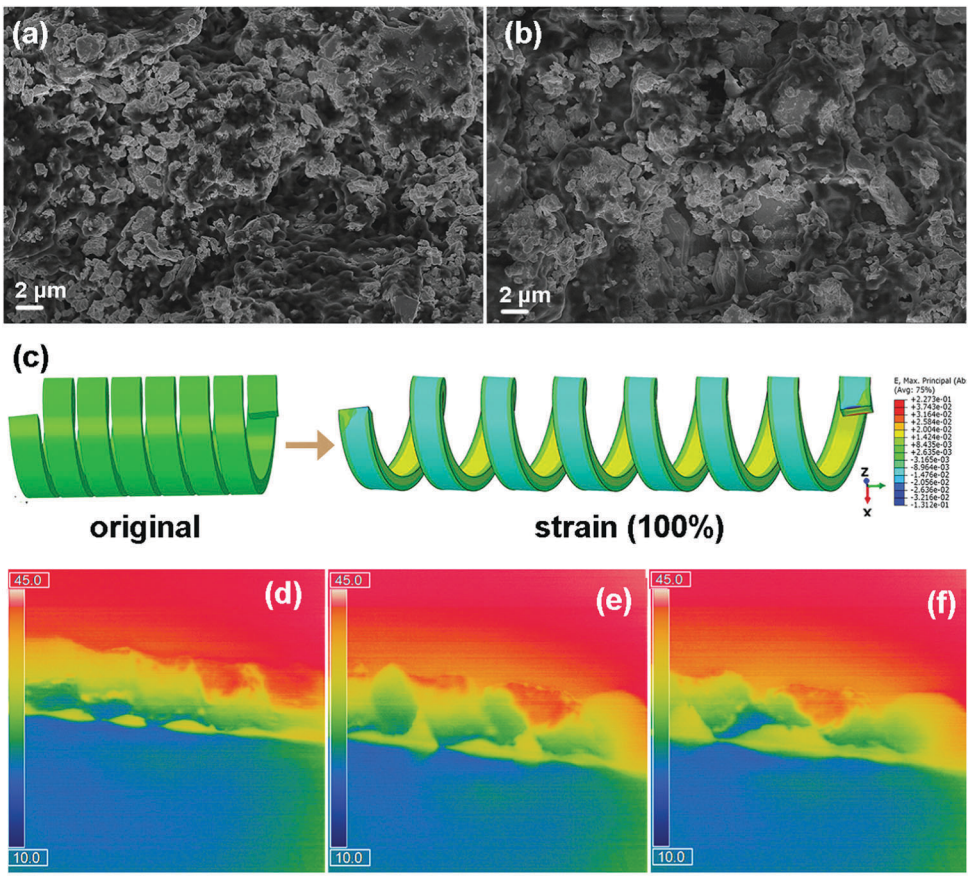

Fig. 3 Morphology, mechanical and thermal analysis of the as-prepared stretchable helical TEG. (a and b) Comparison of the SEM images of a p-type Bi_2Te_3 film before and after cycling tests, respectively. (c) Simulated strain distributions of the helical structure stretched by 100%. (d–f) Thermal images of the stretchable helical TEG under stretching of strains of 0%, $\sim$40%, and $\sim$60%, respectively.

difference of body heat and room temperature (~16 °C) (Fig. 2j). Furthermore, other demonstrations of the flexibility and stretchability of the helical TEG can be seen in Fig. 2k and l. It was rolled into a ring and worn on the finger or applied to the surface of a hot cup with irregular shape, which is nearly impossible for conventional inorganic TE devices. The results verify the great potential of this device as an effective stretchable, breathable and wearable TEG.

To shed light on the stability of the helical TEG under tough mechanical conditions, the morphologies of the active materials on the surface of the helical PU substrate were studied, exemplified by the Bi_2Te_3 film. As shown in Fig. 3a and b, no obvious fractures were observed in the SEM images of the Bi_2Te_3 film before and after the stretching tests (~60% strain, 1000 cycles), which was due to the excellent adhesion between the TE films and substrate. To investigate the root causes of the high stability and reliability of such devices, the local strain distribution of the three-dimensional helical structure under stretching was studied through a Finite Element Analysis (FEA) simulation. As displayed in Fig. 3c (see more details in Movie S1, ESI†), the strain distribution of the helical structure under stretching is very uniform. In other words, no stress concentration which may cause deformations of the active materials is present. More importantly, the surface tension of the helical structure when stretched to 100% remains very low, similar to that of the original state, which is due to the rotation of the three-dimensional helical loop that helps accommodate the mechanical deformations (Movie S2, ESI†). To compare the three-dimensional helical shape with other stretchable architectures,[32–34] a serpentine model under the same mechanical conditions was built (see details in Fig. S10, ESI†). When both structures were stretched by 100%, the local strain of the helical structure was at least an order of magnitude lower than that of the serpentine structure. Thus, it explains a higher level of stretchability of the helical electronic devices. Note that the stretchability of the devices can be easily adjusted by changing the screw diameter and pitch or choosing more elastic polymer substrates.

To understand the thermal distribution of our TEG under stretching, the thermal images of the device under different levels of strains were taken with one side attached to an ice bag and the other left in an ambient atmosphere (Fig. 3d–f). The color gradient along the TE legs indicated the temperature

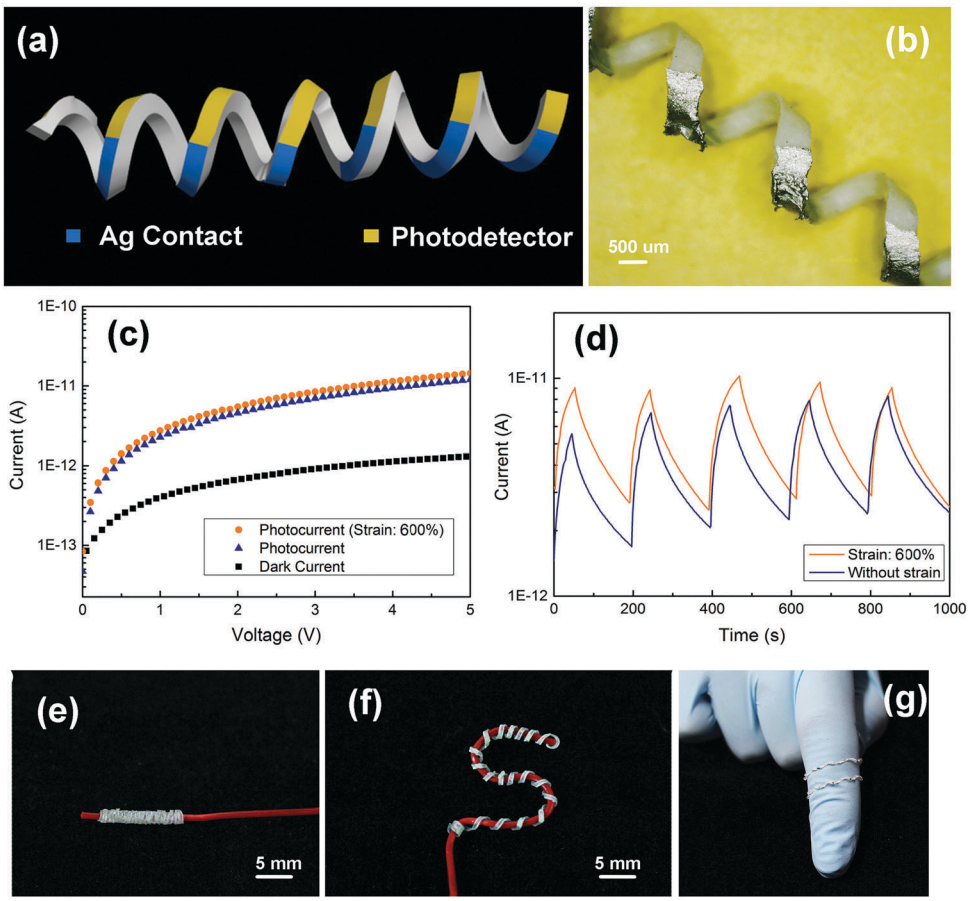

Fig. 4 Optoelectronic performances and demonstrations of the as-prepared highly stretchable helical photodetectors prepared *via* the template method. (a and b) Schematic illustration and photograph of stretchable helical photodetectors, respectively. (c) *I*–*V* characteristics in the dark and under UV illumination in the natural and stretched states. (d) The on–off *I*–*t* characteristics in the natural and stretched states. (e and f) Photographs of a helical photodetector series inserted into a thin electrical wire and reformed into an "S" shape. (g) Photograph of a helical photodetector series worn on a finger. Here they were stretched by ~600%.

difference. From left to right, the color variations remained almost the same when our TEG was stretched from 0% to 60%. In detail, the hollow structure formed between the contact surfaces of heat and cold sources makes it hard for heat to transfer due to the ultra-low thermal conductivity of air ($\sim$0.026 W m^{-1} K^{-1}) and the polymer substrate (PU $\sim$0.22 W m^{-1} K^{-1}).[27,35] This result not only suggests its high stability under deformations but also confirms its great potential as an excellent breathable electronic device because of the gaps between TE loops.

Considering the advantages of the helical structure and the facile template method mentioned above, other polymers, which are typically used as soft substrates in flexible electronic devices, such as poly(ethylene terephthalate) (PET), poly(vinyl alcohol) (PVA) and polydimethylsiloxane (PDMS), can also be exploited to fabricate stretchable and wearable devices (Fig. S5, ESI†). In addition, other rigid inorganic electronic devices, such as photodetectors (PDs)[36] and light emitting diodes (LEDs), can also be made highly stretchable by selecting the suitable polymer substrate and active materials.

For further demonstration of the validity and versatility of this top-down method, ZnO photodetectors (PDs) based on the three-dimensional helical design were presented. Instead of a full coating process, ZnO nanostructures were first grown on the PDMS pre-coated on the screw. Using different seed layers, different ZnO nanostructures would be obtained. With tiny ZnO nanoparticles ($\sim$30 nm) as the seeds, a continuous ZnO nanoaggregate layer would be formed after the hydrothermal synthesis (Fig. S7a, ESI†). However, with a sputtered ZnO thin film as the seed layer, ZnO nanobranch arrays would be grown on a PDMS substrate (Fig. S8, ESI†). To make a PD series, the as-obtained ZnO nanostructures were half-coated with Ag paste and then peeled off (see the Experimental section for more details). Considering the distance between lateral electrodes, the charge collection would be more efficient in a continuous compact film rather than nanoarrays. A higher photocurrent under UV illumination was observed in the compact ZnO nanoaggregate layer than that of the ZnO nanobranch arrays (see details in Fig. S9, ESI†). Therefore, the following study focused on ZnO nanoaggregate film PDs.

The schematic and actual images of the ZnO PDs are shown in Fig. 4a and b, respectively. The stretchable PDs were composed of two parts, *i.e.*, active ZnO material and Ag contacts. In other words, each individual PD was connected with Ag in series. No obvious cracks were observed after the peeling process or under stretching (Fig. S7, ESI†). The optoelectronic properties were investigated on the basis of current–voltage (*I–V*) curves (Fig. 4c). The photocurrent under UV illumination (365 nm, $\sim$1.26 mW cm^{-2}) was approximately an order of magnitude larger than that in the dark. Moreover, compared with the natural state, the photocurrent just showed a slight increase when the PDs were stretched to 600%, mainly due to the larger area exposed to UV light under stretching. The time-dependent on/off photo-response of the inorganic PDs with/without strain was further investigated at a bias of 3 V. As indicated in Fig. 4d, it showed a rapid and stable sensitivity to UV light. The photo-to-dark current ratios of the original and stretched states (up to 600% strain) remained almost unchanged, while previous flexible inorganic electronic devices can typically bear strains of less than 50%.[37–40] Apart from the stretchability, the deformability of the configurable PDs was also demonstrated (Fig. 4e–g). For instance, they can be wrapped twice around a human finger, and easily passed through a wire to be reformed into any shape like "S".

Conclusion

In summary, facing up the challenge of realizing high-performance wearable TEGs, a stretchable and breathable TEG based on a three-dimensional helical design has, for the first time, been demonstrated. This device shows a high stretchability ($\sim$100% strain) and stability (1000 stretching cycles) and air permeability. More importantly, we have presented a novel, facile, effective and versatile "top-down" approach that artfully transforms rigid electronic devices into helical ones. By exploiting this template method, ZnO photodetectors have also been demonstrated as ultra-stretchable ($\sim$600% strain, while most inorganic electronic devices can bear strains of $<$50%), highly deformable and stable. This work provides a promising power source for future wearable electronic devices, and the general and effective method presented here will further help push wearable consumer electronics a step forward.

Conflicts of interest

The authors declare no conflicts of interest.

Acknowledgements

The authors appreciated the helpful discussions and kind support from Kunrong Xu. This work was supported by MOST (2016YFA0203302), NSFC (21634003, 11674061, 51471051, 51573027, 51403038, 51673043, 21604012, 21503079), STCSM (16JC1400702, 17QA1400400, 15XD1500400, 15JC1490200) and SHMEC (2017-01-07-00-07-E00062).

Notes and references

1 D.-H. Kim, J.-H. Ahn, W. M. Choi, H.-S. Kim, T.-H. Kim, J. Song, Y. Y. Huang, Z. Liu, C. Lu and J. A. Rogers, *Science*, 2008, **320**, 507–511.
2 D.-Y. Khang, *Science*, 2006, **311**, 208–212.
3 C.-C. Kim, H.-H. Lee, K. H. Oh and J.-Y. Sun, *Science*, 2016, **353**, 682–687.
4 J. Y. Oh, S. Rondeau-Gagné, Y.-C. Chiu, A. Chortos, F. Lissel, G.-J. N. Wang, B. C. Schroeder, T. Kurosawa, J. Lopez, T. Katsumata, J. Xu, C. Zhu, X. Gu, W.-G. Bae, Y. Kim, L. Jin, J. W. Chung, J. B.-H. Tok and Z. Bao, *Nature*, 2016, **539**, 411–415.
5 W. Gao, S. Emaminejad, H. Y. Y. Nyein, S. Challa, K. Chen, A. Peck, H. M. Fahad, H. Ota, H. Shiraki, D. Kiriya, D.-H. Lien, G. A. Brooks, R. W. Davis and A. Javey, *Nature*, 2016, **529**, 509–514.

6 T. Leydecker, M. Herder, E. Pavlica, G. Bratina, S. Hecht, E. Orgiu and P. Samorì, *Nat. Nanotechnol.*, 2016, **11**, 769–775.
7 J. A. Rogers, T. Someya and Y. Huang, *Science*, 2010, **327**, 1603–1607.
8 B. Y. Ahn, E. B. Duoss, M. J. Motala, X. Guo, S.-I. Park, Y. Xiong, J. Yoon, R. G. Nuzzo, J. A. Rogers and J. A. Lewis, *Science*, 2009, **323**, 1590–1593.
9 T. Someya, Z. Bao and G. G. Malliaras, *Nature*, 2016, **540**, 379–385.
10 N. Matsuhisa, D. Inoue, P. Zalar, H. Jin, Y. Matsuba, A. Itoh, T. Yokota, D. Hashizume and T. Someya, *Nat. Mater.*, 2017, **16**, 834–840.
11 Y. Sun, V. Kumar, I. Adesida and J. A. Rogers, *Adv. Mater.*, 2006, **18**, 2857–2862.
12 W. M. Choi, J. Song, D. Y. Khang, H. Jiang, Y. Y. Huang and J. A. Rogers, *Nano Lett.*, 2007, **7**, 1655–1663.
13 Y. Chen, Y. Zhao and Z. Liang, *Energy Environ. Sci.*, 2015, **8**, 401–422.
14 H. Wu, Y. Huang, F. Xu, Y. Duan and Z. Yin, *Adv. Mater.*, 2016, **28**, 9881–9919.
15 C. Yang, D. Souchay, M. Kneiß, M. Bogner, H. M. Wei, M. Lorenz, O. Oeckler, G. Benstetter, Y. Q. Fu and M. Grundmann, *Nat. Commun.*, 2017, **8**, 16076.
16 S. L. Kim, K. Choi, A. Tazebay and C. Yu, *ACS Nano*, 2014, **8**, 2377–2386.
17 S. Li, W. Peng, J. Wang, L. Lin, Y. Zi, G. Zhang and Z. L. Wang, *ACS Nano*, 2016, **10**, 7973–7981.
18 A. K. Bansal, S. Hou, O. Kulyk, E. M. Bowman and I. D. W. Samuel, *Adv. Mater.*, 2015, **27**, 7638–7644.
19 S. J. Kim, J. H. We and B. J. Cho, *Energy Environ. Sci.*, 2014, **7**, 1959–1965.
20 F. Kim, B. Kwon, Y. Eom, J. E. Lee, S. Park, S. Jo, S. H. Park, B.-S. Kim, H. J. Im, M. H. Lee, T. S. Min, K. T. Kim, H. G. Chae, W. P. King and J. S. Son, *Nat. Energy*, 2018, **3**, 301–309.
21 X. Xu, J. Bullock, L. T. Schelhas, E. Z. Stutz, J. J. Fonseca, M. Hettick, V. L. Pool, K. F. Tai, M. F. Toney, X. Fang, A. Javey, L. H. Wong and J. W. Ager, *Nano Lett.*, 2016, **16**, 1925–1932.
22 B. Poudel, Q. Hao, Y. Ma, Y. Lan, A. Minnich, B. Yu, X. Yan, D. Wang, A. Muto, D. Vashaee, X. Chen, J. Liu, M. S. Dresselhaus, G. Chen and Z. Ren, *Science*, 2008, **320**, 634–638.
23 G. J. Snyder and E. S. Toberer, *Nat. Mater.*, 2008, **7**, 105–114.
24 T. Zhu, Y. Liu, C. Fu, J. P. Heremans, J. G. Snyder and X. Zhao, *Adv. Mater.*, 2017, **14**, 1605884.
25 Z. Liu, J. Mao, J. Sui and Z. Ren, *Energy Environ. Sci.*, 2017, **11**, 23–44.
26 S. H. Jeong, F. J. Cruz, S. Chen, L. Gravier, J. Liu, Z. Wu, K. Hjort, S. L. Zhang and Z. Bin Zhang, *ACS Appl. Mater. Interfaces*, 2017, **9**, 15791–15797.
27 J. P. Rojas, D. Singh, D. Conchouso, A. Arevalo, I. G. Foulds and M. M. Hussain, *Nano Energy*, 2016, **30**, 691–699.
28 S. Xu, Z. Yan, K.-I. Jang, W. Huang, H. Fu, J. Kim, Z. Wei, M. Flavin, J. McCracken, R. Wang, A. Badea, Y. Liu, D. Xiao, G. Zhou, J. Lee, H. U. Chung, H. Cheng, W. Ren, A. Banks, X. Li, U. Paik, R. G. Nuzzo, Y. Huang, Y. Zhang and J. A. Rogers, *Science*, 2015, **347**, 154–159.
29 M. Ito, T. Koizumi, H. Kojima, T. Saito and M. Nakamura, *J. Mater. Chem. A*, 2017, **5**, 12068–12072.
30 W. Liu, H. S. Kim, Q. Jie and Z. Ren, *Scr. Mater.*, 2016, **111**, 3–9.
31 Z. Liu, Y. Wang, J. Mao, H. Geng, J. Shuai, Y. Wang, R. He, W. Cai, J. Sui and Z. Ren, *Adv. Energy Mater.*, 2016, **6**, 1–11.
32 P. Gutruf, S. Walia, M. Nur Ali, S. Sriram and M. Bhaskaran, *Appl. Phys. Lett.*, 2014, **104**, 1–5.
33 A. J. Bandodkar, I. Jeerapan, J. M. You, R. Nuñez-Flores and J. Wang, *Nano Lett.*, 2016, **16**, 721–727.
34 T. Cheng, Y. Zhang, W. Y. Lai and W. Huang, *Adv. Mater.*, 2015, **27**, 3349–3376.
35 Y.-M. Ha, D. Lim, S. Y. Lee, J. Kim, J. H. Kim, Y. A. Kim and Y. C. Jung, *Macromol. Res.*, 2017, **25**, 1015–1021.
36 X. Xu, S. Shukla, Y. Liu, B. Yue, J. Bullock, L. Su, Y. Li, A. Javey, X. Fang and J. W. Ager, *Phys. Status Solidi RRL*, 2017, **4**, 1700381.
37 A. Miyamoto, S. Lee, N. F. Cooray, S. Lee, M. Mori, N. Matsuhisa, H. Jin, L. Yoda, T. Yokota, A. Itoh, M. Sekino, H. Kawasaki, T. Ebihara, M. Amagai and T. Someya, *Nat. Nanotechnol.*, 2017, **12**, 907–913.
38 S.-T. Han, H. Peng, Q. Sun, S. Venkatesh, K.-S. Chung, S. C. Lau, Y. Zhou and V. A. L. Roy, *Adv. Mater.*, 2017, **29**, 1700375.
39 M. Choi, B. Jang, W. Lee, S. Lee, T. W. Kim, H.-J. Lee, J.-H. Kim and J.-H. Ahn, *Adv. Funct. Mater.*, 2017, **27**, 1606005.
40 P. Gutruf, E. Zeller, S. Walia, H. Nili, S. Sriram and M. Bhaskaran, *Small*, 2015, **11**, 4532–45839.

